Selective electrocatalytic upgrading of lignin to aryl aldehydes and carboxylic acids over dodecyl sulfate-intercalated CoS nanocones

Zhiyong Fang [a], Fuhua Li [b], Mei Wang [a], Fusheng Li [a], Xiujuan Wu [a], Ke Fan [a], Qing Tang [b,*], Licheng Sun [a,c], Peili Zhang [a,*]

[a] State Key Laboratory of Fine Chemicals, Institute of Artificial Photosynthesis, DUT-KTH Joint Education and Research Centre on Molecular Devices, Dalian University of Technology, Dalian 116024, PR China
[b] School of Chemistry and Chemical Engineering, Chongqing Key Laboratory of Theoretical and Computational Chemistry, Chongqing University, Chongqing 401331, PR China
[c] Center of Artificial Photosynthesis for Solar Fuels, School of Science, Westlake University, Hangzhou 310024, PR China

A R T I C L E   I N F O

A B S T R A C T

Lignin is the biggest and most sustainable reservoir for aromatics, but its selective degradation is still a challenge. Herein, we report the electrocatalytic cleavage of the C_α-C_β bonds of β-O-4, a lignin model, under mild conditions using a dodecyl sulfate-intercalated cobalt sulfide (DS-CoS) nanocone catalyst. With this noble-metal-free nanocones as an electrocatalyst, β-O-4 can be selectively oxidized to the corresponding aldehydes or carboxylates in excellent yields (90–97%) by control potential electrolysis. Moreover, the electrochemical upgrading of lignin produces aryl aldehydes or carboxylic acids in yields of 21.4 and 23.9 wt%, respectively, by controlling potential electrolysis. Mechanism studies show that the hydroxyl radicals electrogenerated on the surface of the $SCo^{3+}OH$ intermediate induce the cleavage of C_α-C_β bonds to form aldehydes, which are further oxidized to carboxylic acids by superoxide radicals electrogenerated on the surface of the Co^{4+} intermediate. This approach features the merits of low-cost and good stability of the electrocatalyst, high conversion of β-O-4, high selectivity of products, and mild reaction conditions.

1. Introduction

Lignin composed of a series of phenylpropane units is a major natural source of aromatic chemicals [1–10]. Therefore, the depolymerization of lignin is believed to be a sustainable approach for aryl monomers, which can reduce our dependence on limited fossil fuel energy and chemical sources. The major link units in lignin are categorized into seven types, as shown in Scheme 1a: β-O-4 (β-aryl ether), $\beta - \beta$ (resinol), β-5 (phenylcoumaran), α-O-4 (α-arylether), 4-O-5 (diaryl ether), $5 - 5'$ (biphenyl), and β-1 (β-aryl alcohol). Among them, β-O-4 is the richest unit of native lignin, accounting for 43–56%. Hence, the cleavage of β-O-4 is important for lignin upgrading. However, to date, the C(OH)–C cleavage remains underexplored, probably because of its high bond dissociation energy (260–300 kJ mol^{-1}) [5–7].

Electrocatalytic oxidation using renewable energy-generated power is an attractive approach for lignin depolymerization, which allows product control [11–18]. As shown in Scheme 1b, the C_α–C_β bond of β-O-4 can be oxidatively cleavaged to aromatic aldehydes and carboxylic acids by electrocatalysis under mild conditions [19–21]. Pardini and co-workers first reported the electrocatalytic oxidation of β-O-4 with a bulk Ni electrode at 150–160 °C, but only 20.9% yield of aromatic aldehydes and carboxylic acids was obtained [22]. Since then, transition metal catalysts (Ni, PbO$_2$, and TiO$_2$) [23–32], precious metal catalysts (Pt, RuO$_2$, and IrO$_2$) [33–42], and single-atom catalysts (Pt$_1$/N-CNTs) [43] have been reported for depolymerization of lignin and its model compounds (Scheme 1c). Stahl and co-workers reported an indirect electrooxidation method using 2,2,6,6-tetramethyl-1-piperidine-*N*-oxyl (TEMPO) and its derivatives as redox mediators to facilitate C_α−C_β cleavage, resulting in a slightly higher yield (7–9%) of aromatic monomers[44]. However, the use of organic redox mediators, such as TEMPO [44,45], 2,2′-azinobis(3-ethylbenzthiazoline-6-sulfonate) (ABTS) [46,47], and 1-hydroxybenzotriazole (HBT) [46,47], makes product separation difficult. Currently, the electrocatalytic lignin oxidation via selective C–C cleavage is still at a preliminary stage and remains a challenge. There are several critical bottlenecks, including the high cost of the catalysts [33–43], the need for sacrificial oxidants [35,

43], poor selectivity [28–33,48], and low product yields [27–32,41, 48–51]. In this context, the development of environmentally friendly and efficient alternative strategies for the selective cleavage of C−C bonds to upgrade lignin under mild conditions is required. Moreover, the utilization efficiency of electric energy can be enhanced by coupling the oxidative cleavage to a reductive half-reaction, such as reductive cleavage reaction, H_2 evolution, or other electrochemical reduction reactions [22–25].

Herein, we report an electrochemical oxidation approach for the selective upgrading of β-O-4 and, by extension, of lignin to small-molecule aromatic compounds over a dodecyl sulfate-intercalated cobalt sulfide nanocone (denoted as DS-CoS NC) catalyst in basic aqueous solution at room temperature in the absence of chemical oxidants (Scheme 1d). The as-prepared catalyst selectively catalyzed the C_α-C_β

cleavage of β-O-4 to form the corresponding aromatic aldehydes and carboxylates at 1.05 and 1.45 V vs. the reversible hydrogen electrode (RHE), respectively. Our investigation revealed that the mechanism for the C-C cleavage involves tandem OH-radical-induced oxidation, resulting in the production of aromatic aldehydes. Upon increasing the applied potential over 1.25 V vs. RHE, the aldehydes were further oxidized to carboxylates by superoxide radicals. Overall, the results of this work demonstrated that the DS-CoS catalyst is highly efficient for the electrochemical oxidation of β-O-4 to aromatic aldehydes ($\geq$ 90% yield at 1.05 V vs. RHE) and aromatic carboxylates ($\geq$ 94% yield at 1.45 V vs. RHE). In addition, the electrolysis of lignin at 1.05 and 1.45 V vs. RHE achieved a yield of 21.4 wt% for aromatic aldehydes and 23.9 wt% for aromatic carboxylates, respectively.
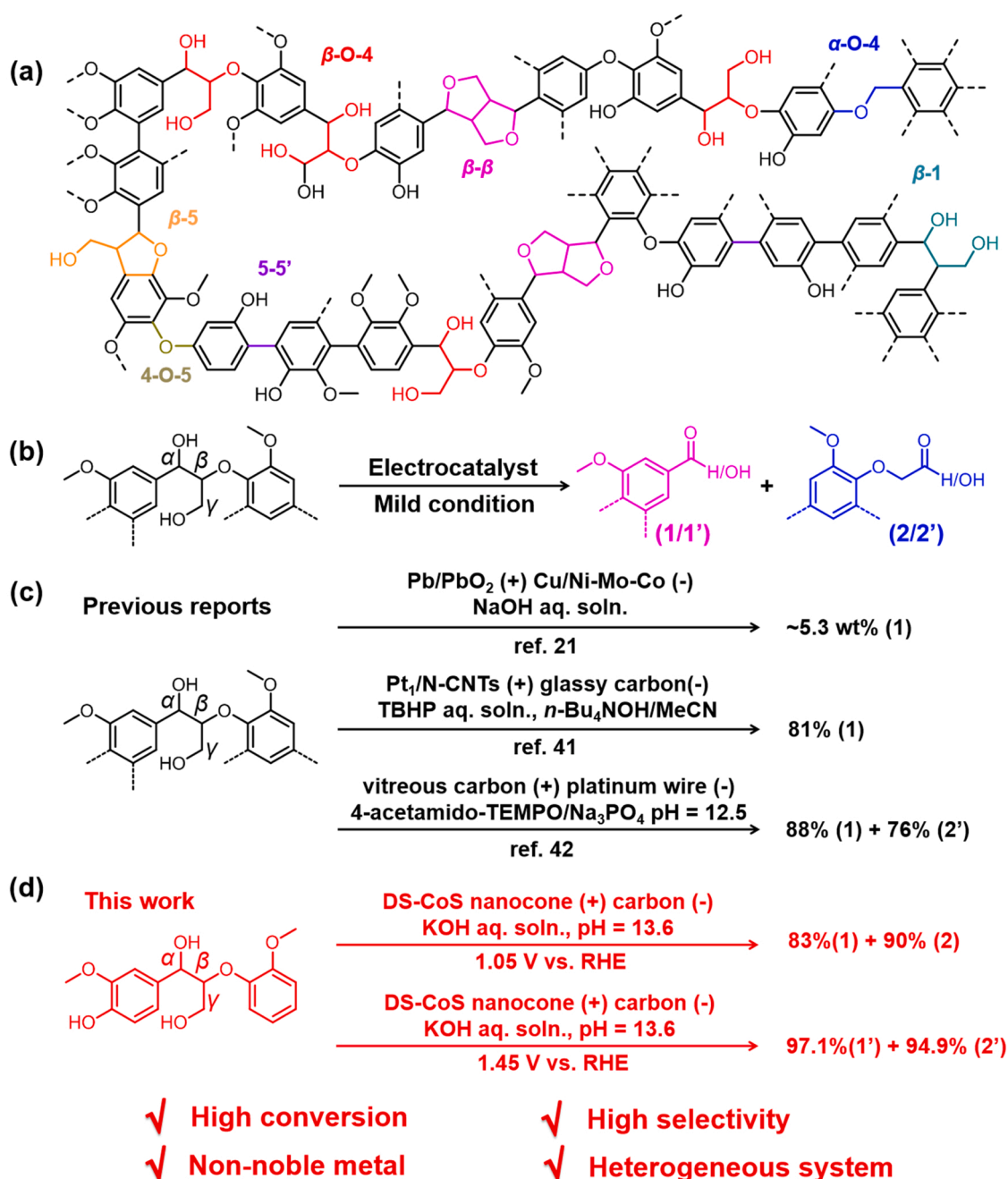
Scheme 1. (a) A representative structure of lignin. (b) Electrochemical oxidation of the lignin model compound β-O-4. (c) Previously reported electrocatalytic systems for β-O-4 oxidation. (d) The electrocatalytic systems developed in this work, with DS-CoS as an electrocatalyst under ambient conditions.

2. Experimental methods

2.1. Solvents and reagents

The chemicals and solvents were purchased from commercially available sources and used without further purification. As the commercial p-benzoquinone also contains p-phenol, the KOH solution of purchased p-benzoquinone was electrochemically oxidized at 1.5 V vs. RHE for 30 min prior to use. The lignin model β-O-4 was synthesized according to previously reported procedures and the ^{1}H and ^{13}C NMR spectra were shown at the end of the article (Fig. S20) [52–55].

2.2. Synthesis of the DS-CoS nanocones

The synthesis of DS-CoS nanocone refers to previous literature and the experimental process was improved on this basis [56–59]. The chloride hexahydrate (CoCl$_2$0.6 H$_2$O), sodium dodecyl sulfate (SDS) and hexamethylenetetramine (HMT) were dissolved in deionized water with concentrations of 6 mM, 25 mM and 20 mM respectively. The mixture solution was stirred at 95 °C for 6 h with Ar. The solution changed from pink to green, and got a suspension with green particles finally. The product was centrifuged, washed with deionized water and ethanol several times, and dried at 60 °C overnight under vacuum. The resulting green powder (0.5 g) and sublimated sulfur (0.1 g) were placed in two separate porcelain boats in a furnace, respectively, and the boat with sulfur was at the upstream side. The materials were annealed at 300 °C for 2 h, and the DS-CoS nanocone was obtained. The synthesis method of CoS without anions of dodecyl sulfate was the same as the above, except that there is no participation of sodium dodecyl sulfate. The layer spacing of as-synthesized DS-CoS nanocone was calculated using the following equations (d$_{(00 L)}$, the crystal plane distance of (00 L), d, the layer spacing of DS-CoS):

$$2d_{(00L)}\sin\theta_{(00l)} = n\lambda (L=1,2\cdots7, n = 1, \lambda = 0.15406 \text{ nm, Cu K}\alpha1 \text{ was used}) \quad (1)$$

$$d = 1/7(1{\times}d(001) + 2{\times}d(002) + 3{\times}d(003) + 4{\times}d(004) + 5{\times}d(005) + 6{\times}d(006) + 7{\times}d(007)) \quad (2)$$

2.3. Characterizations

X-ray photoelectron spectroscopy (XPS) was performed using a Thermo ESCALAB XI+ surface analysis system. Powder X-ray diffraction (XRD) data were acquired with a Bruker D8 Advance. Scanning electron microscope (SEM) images and energy dispersive X-ray (EDX) spectra were obtained with a HITACHI UHR FE-SEM SU8220 and JEOL JSM 7401 equipped with an EDX system. Transmission electron microscope (TEM) images were acquired using a JEOL JEM2100 instrument. Raman spectrum data were obtained with a Renishaw inVia Qontor. Infrared spectroscopy (IR) spectrum was conducted by Thermo Nicolet IS50. Electron paramagnetic resonance (EPR) data were acquired with a Bruker A200–9.5/12.

2.4. Electrochemical measurements

The electrochemical behavior was carried out with a CH Instrument 660E potentiostat. The electrochemical cell contained the sample as a working electrode (WE), a carbon rod as an auxiliary electrode (AE), and Hg/HgO (1 M KOH, Aida) as a reference electrode ($E°_{Hg/HgO}$ = 0.098 V vs. SHE). The DS-CoS nanocone (5 mg) and Nafion117 solution (50 μl) were dispersed in ethanol (1 ml), and sonicated for 40 min. Then, the suspension was evenly spread on the surface of carbon paper, which was pre-treated with nitric acid, acetone, and deionized water. The catalyst loading was determined to be 1.0 ± 0.1 mg cm^{-2} eventually. The electrolyte solution is 1 M KOH in 30 ml aqueous solution. The reference electrodes (RE) were calibrated by measuring the standard hydrogen

electrode (SHE) potential. Potentials were converted to reversible hydrogen electrode (RHE) via the Nernst equation: $E_{RHE} = E_{Hg/HgO}$ + 0.059 pH + $E°_{Hg/HgO}$. The chronoamperometry of β-O-4 and lignin were conducted by DS-CoS nanocone as WE with electrode area of 5 cm^2 in 30 ml of electrolyte solution. In the experiment of isotope tracing, the water of ^{18}O (99.5%) is used instead of ordinary water as the electrolyte solvent. The constant potential electrolysis of p-benzoquinone was carried out with glass carbon as WE. The Faradaic efficiency (FE) values for the electrochemical oxidation of β-O-4 were calculated using the following equations (F, Faraday's constant, 96,485.33289 $\pm$ 0.00059 C mol^{-1}):

$$\text{Faradaic efficiencies} = \frac{\text{mol of aldehyde formed}}{\text{Total charge passed } /(2 \times \text{F})} \times 100\% \quad (3)$$

$$\text{Faradaic efficiencies} = \frac{\text{mol of acid formed}}{\text{Total charge passed } /(6 \times \text{F})} \times 100\% \quad (4)$$

Analysis of the oxidation products of β-O-4 and lignin were performed using a Shimadzu Prominence high-performance liquid chromatography (HPLC) system equipped with an SPD-M20A diode array detector and a 4.6 mm × 150 mm Shim-pack GWS 5 μm C-18 column at 40 °C. HPLC eluents for the chronoamperometry of β-O-4 were mixtures of H$_2$O (0.1% H$_3$PO$_4$) and CH$_3$OH with a ratio of 4:6, and CH$_3$OH: DMSO = 9: 1 for lignin and its oxidation products with internal standard (IS) of 1,4-dimethoxybenzene. The concentration range of calibration curve: 1–20 mM. The wavelength for analysis: 280 nm, the calibration plots are shown in Fig. S15. 2D ^{1}H−^{13}C HSQC NMR spectra of the lignin before and after oxidation were obtained on a Bruker Avance-600 MHz NMR spectrometer with residual solvent peaks (D-DMSO) as the internal reference. Gel permeation chromatography (GPC) characterization of lignin polymer and its oxidation products were conducted using a PSS PolarSil Linear S column with a solution of dimethyl formamide (DMF) as the mobile phase, sample concentration: 1.00 mg ml^{-1}, injection volume: 10.0 μl. The calibration curve: y = 331.557370 − 230.327982x + 65.565103x^2 − 9.326074x^3 + 0.659675x^4 − 0.018552x^5. High Limit MW RT: 5.99 min, Low Limit MW RT: 8.63 min

The electron spin resonance (ESR) analysis is carried out to detect the spin reactive ●OH and ●O2$^-$ species on the catalyst surface and/or dissolved in electrolyte by using 5,5-dimethyl-1-pyrroline N-oxide (DMPO) as a spin trap. The ESR experiments are conducted in two methods. Firstly, electrolysis with DMPO before sampling. Control the chronoamperometry experiment at 1.05 and 1.45 V vs. RHE for 10 min with 10 mg DMPO in 30 ml electrolyte, respectively. Then, take a sample of 1 ml electrolyte for ESR tests. Secondly, conducted the chronoamperometry experiment at 1.05 and 1.45 V vs. RHE without DMPO. Take samples of 1 ml electrolyte, then add DMPO into the samples for ESR tests.

2.5. Computational details

All density functional theory (DFT) calculations are performed in the standard Gaussian 16 software package [60]. The geometry optimization, vibrational frequency, transition state (TS) search and intrinsic reaction coordinate (IRC) are carried out by using the B3LYP-D3(BJ) [61,62] (including London-dispersion correction) functional with the 6–311 +G(d) basis set for all atoms. The vibrational frequency calculations are subsequently carried out at the same level as geometry optimizations for two purposes, 1) characterizing the nature of the stationary point that all frequencies of local minimum are positive and the first-point saddle point (i.e. transition state (TS) has only one imaginary frequency; 2) obtaining the thermodynamic quantities of the studied species at 363.15 K and 0.1 MPa such as relative Gibbs free-energies. IRC calculations are used to track the selected transition structures for ensuring their connectivity of reactant complexes (RC) and intermediate or product complexes (PC). In addition, the

single-point energy of stationary point is calculated based on the B3LYP-D3(BJ) functional with the def2-TZVP basis set for all atoms. In order to facilitate the comparison of activation energy barriers of different reaction pathways, we assume the Gibbs free energy of the RC as the respective reference value (zero) for different pathways.

3. Results and discussions

3.1. Characterization of the DS-CoS nanocones

The as-prepared DS-CoS NCs were characterized by XRD, TEM, Fourier transform infrared (FT-IR) spectroscopy, and XPS. The XRD pattern of the DS-CoS nanocones contains diffraction peaks at 30.54°, 35.26°, 46.97°, and 54.28° (Fig. 1a), which match the standard pattern of CoS (JCPDS#75–0605). Furthermore, a low-index diffraction peaks was observed in the range of 0–20°, corresponding to an interlayer distance of 2.5 nm. Next, the morphology of the DS-CoS NCs were studied by TEM.

Fig. 1b shows that the as-prepared DS-CoS nanocones have a bottom diameter of 100 ± 20 nm and a height of 300 ± 30 nm. The high-resolution (HR)-TEM image of the DS-CoS NCs shows lattice fringes with planar spacings of 0.169, 0.193, and 0.292 nm, corresponding to (110), (102), and (100) crystal planes, respectively (Fig. 1c). The energy dispersive X-ray spectroscopy elemental mapping images (EDS) of the DS-CoS nanocones are displayed in Fig. 1d, which illustrates the homogeneous distribution of Co, S, C, and O. Moreover, the bands corresponding to the vibrations of interlayer anions were observed in the FT-IR spectra (Fig. S1). In particular, the asymmetric and symmetric CH_2 stretching vibrations at 2924 and 2849 cm^{-1} are ascribed to the alkyl chains of dodecyl sulfate, and the relatively weak band at 2965 cm^{-1} is due to the stretching vibration of the terminal CH_3 group of the hydrocarbon tail. Besides, the series of bands at 1300–900 cm^{-1} corresponds to the stretching mode of sulfate ($-OSO_3^-$). The XPS survey spectrum confirms the presence of Co, C, O, and S in the as-prepared catalyst (Fig. S2). The Co 2p XPS profile contains a peak at the binding energy of 780.93 eV (Co $2p_{3/2}$), which can be assigned to the Co^{2+} in
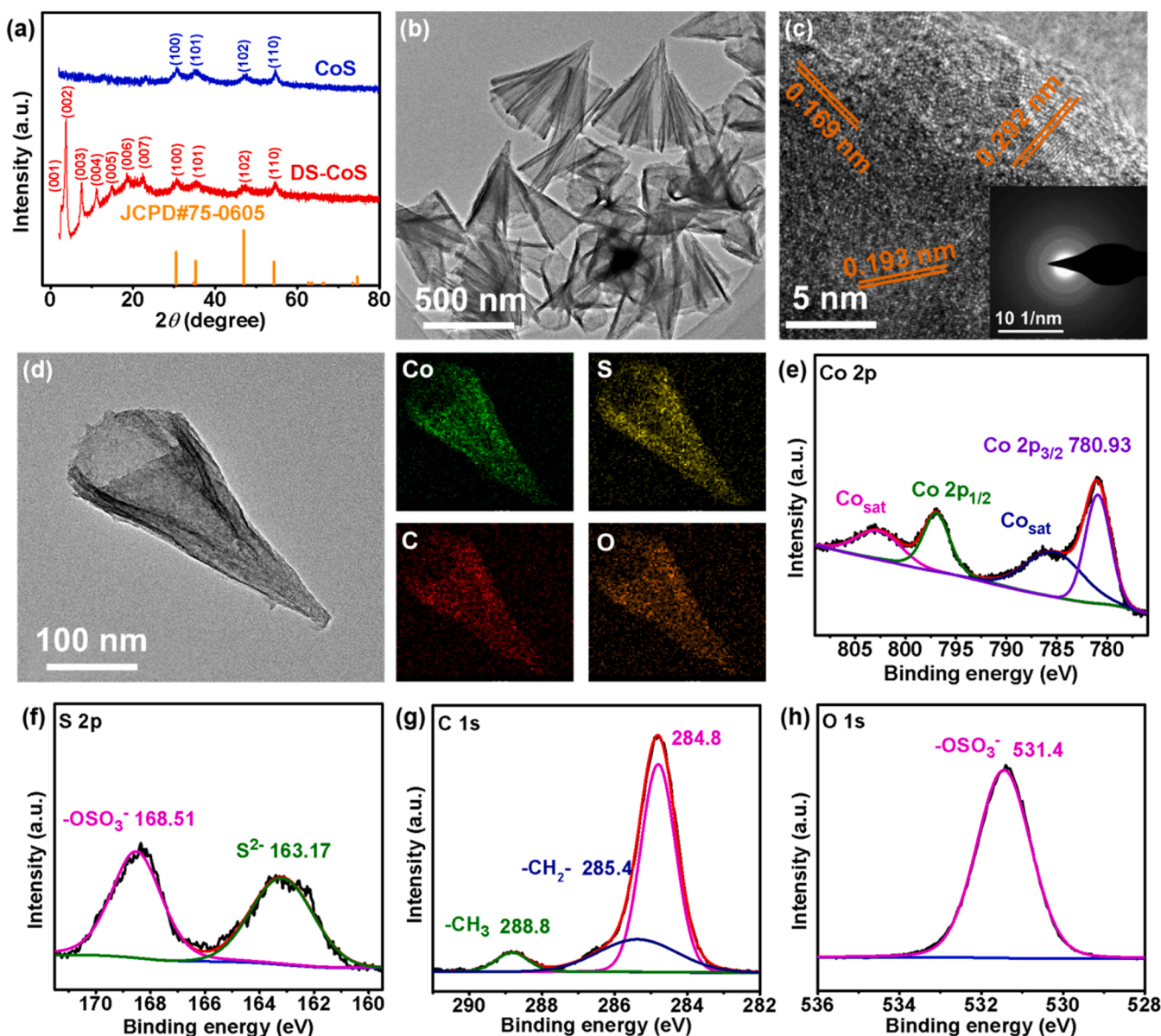

Fig. 1. (a) XRD patterns of the DS-CoS nanocones and CoS. (b) TEM image of DS-CoS nanocones. (c) HR-TEM image of DS-CoS nanocones. The inset in (c) shows the selected area electron diffraction pattern of the DS-CoS nanocones. (d) TEM and EDS elemental mapping images of DS-CoS nanocones. (e-h) XPS spectra of (e) Co $2p$, (f) S $2p$, (g) C $1s$, and (h) O $1s$ obtained for the DS-CoS nanocones.

DS-CoS (Fig. 1e). The S 2*p* XPS spectrum in Fig. 1f can be fitted by two peaks at 168.51 eV and 163.17 eV, ascribed to the S species of -OSO$_3^-$ and S^{2-} moieties, respectively. Besides, the O 1 *s* peak at 531.45 eV can be assigned to $-$OSO$_3^-$, and the C 1 *s* peaks at 288.82 and 285.37 eV are assigned to -CH$_3$ and -CH$_2$-, respectively (Fig. 1g,h).

3.2. Electrocatalytic oxidation of β-O-4

The performance of the DS-CoS nanocone catalyst for the cleavage of C-C bonds was initially studied with a representative dimeric model of β-O-4, which contains C$_\alpha$-OH, C$_\alpha$-C$_\beta$, and C$_\beta$-O bonds. Cyclic voltammetry and chronoamperometry experiments were conducted in a 1 M KOH aqueous solutions. The cyclic voltammogram (CV) of DS-CoS NCs in 1 M KOH shows a Co$^{2+/3+}$ oxidation peak at 1.05 V vs. RHE, followed.

by the oxygen evolution reaction (OER) peak beyond 1.53 V vs. RHE (Fig. 2a). When 10 mM β-O-4 was added to the electrolyte solution, the current density showed an obvious enhancement just after the Co$^{2+/3+}$ oxidation process, which can be attributed to the β-O-4 oxidation reaction (Fig. 2a, red line). Control experiments with a glassy carbon plate showed a Faradaic silent region before 1.5 V vs. RHE, both with and without β-O-4 (Fig. 2b). These results indicate that the oxidation of β-O-4 is electrocatalyzed by the DS-CoS nanocones.

The electrocatalytic property of DS-CoS NCs toward the oxidation of β-O-4 was further studied via chronoamperometry measurements at 1.05 and 1.45 V vs. RHE. The.

conversion and Faradaic efficiency were determined by high-performance liquid chromatography (HPLC) and electroanalytical methods. After electrolysis at 1.05 V vs. RHE for 5 h, the current was close to 0, and the accumulated charge reached 69 C (Fig. 2c). The conversion of β-O-4 was 96%, and the total Faradaic efficiency was 83.6%. Fig. 2d and S3 show the changes in the concentration of β-O-4 and its oxidation products versus time during the electrolysis process. The major products, identified by HPLC analysis, were vanillin (V-aldehyde), 2-methoxyphenoxyacetic aldehyde (M-aldehyde), and guaiacol with yields of approximately 83%, 90%, and 4.4%, respectively, indicating C$_\alpha$-C$_\beta$ cleavage (Fig. 2e). The selectivities of V-aldehyde and M-aldehyde went up to 90% and 96%, respectively, when the electrolyte concentration of KOH was decreased to 0.1 M (Fig. S4). Additionally, vanillyl alcohol (V-alcohol), vanillic acid (V-acid), 2-methoxyphenoxyacetic alcohol (M-alcohol), and 2-methoxyphenoxy-acetic acid (M-acid) were detected as byproducts of the Cannizzaro reaction of aldehydes in alkaline aqueous solution. Interestingly, the chronoamperometry at 1.45 V vs. RHE yielded different products. After electrolysis at 1.45 V vs. RHE for 3.5 h, the cumulative charges reached 177 C (Fig. 2f). The conversion and total Faradaic efficiency were about 98% and 87.2%, respectively. HPLC analysis confirmed that the major products were V-acid, M-acid, and guaiacol with yields of 97.1%, 94.9%, and 4.5%, respectively, together with a very small amount of not further oxidized intermediates, V-aldehyde and M-aldehyde (Figs. 2g and S5). These results indicate that the electrocatalytic oxidation of β-O-4 at 1.45 V vs. RHE involves a two-step process including C$_\alpha$-C$_\beta$ cleavage and the further oxidation reactions (Fig. 2h). Next, chronoamperometry measurements at various potentials were conducted to investigate the scopes of applied potentials for C$_\alpha$-C$_\beta$ cleavage and further oxidation (Fig. S6a, b). The results showed that the C$_\alpha$-C$_\beta$ cleavage started at 0.95 V vs. RHE, and the reaction rate gradually accelerated with increase in applied potential. When the potential exceeded 1.25 V vs. RHE, V-acid and M-acid were detected, indicating a further oxidation of the aromatic aldehydes formed in the first step.

The stability of the DS-CoS NCs for β-O-4 oxidation was studied by continually repeating the electrolysis at 1.45 V vs. RHE five times. The conversions, Faradaic efficiencies, and the yields and selectivities of products were all maintained, indicating a stable catalytic performance under testing conditions (Fig. S7a). After the continual electrolysis, the working electrode was characterized by XRD, TEM, and IR (Fig. S7b–d). The used DS-CoS nanocone catalyst displayed an XRD pattern similar to

that of the as-prepared catalyst in terms of its layered structure and interplanar spacing (Fig. S7b). Additionally, the morphology of the nanocones remained unchanged (Fig. S7c), and the IR spectrum indicated that dodecyl sulfate anions were still embedded in the layered structure (Fig. S7d). Overall, the results indicated that the DS-CoS nanocone catalyst was stable during the electrocatalytic oxidation of β-O-4 under testing conditions.

More cobalt-based catalysts, including Co(OH)$_2$, CoO, Co$_3$O$_4$, CoS, and CoSe, were tested for comparison. Under the same conditions, the DS-CoS nanocones exhibited the best performance for the electro-oxidation of β-O-4, probably resulting from its unique nanostructure (Fig. S8). Compare with the previous reports, DS-CoS NCs show one of the best selectivity for aromatic aldehydes or aromatic acids, respectively (Table S1). And the selectivity shows very good controllability by turning the applied potentials. To the best of our knowledge, this kind of controlled, highly selective, and oxidant-free catalytic system for β-O-4 oxidation cleavage has been rarely reported.

3.3. Electrochemical processes on the surface of the DS-CoS nanocones

Previous reports have shown that the distinct intermediates electrogenerated at various applied potentials induce the oxidation of a target substrate to yield different products [63–66]. In this study, the electrooxidation of β-O-4 on the DS-CoS nanocones produced different products at 1.05 and 1.45 V vs. RHE. Therefore, it is reasonable to infer that the electrogenerated intermediates at the corresponding potentials are different.

Thus, the electrogenerated active species on the working electrode surface were investigated by in situ electrochemical/Raman spectroscopy (IERS) and open circuit potential–time (OCPT) measurements. As shown in Fig. 3a, at 0.90 V vs. RHE, the DS-CoS NCs displayed peaks at 468, 511, and 668 cm^{-1}, attributed to the E$_g$, F$_{2 g}$, and A$_{1 g}$.

vibrational modes of Co$=$S, respectively [67–69]. When the applied potential exceeded 0.95 V vs. RHE, a new peak at 679 cm^{-1} was observed, and it can be unambiguously assigned to Co^{3+}, which is consistent with the Co$^{2+/3+}$ oxidation peak detected by cyclic voltammetry. The A$_{1 g}$ peak (679 cm^{-1}) corresponding to Co^{3+} went up with the increase in the potential, while the peak at 668 cm^{-1} for the Co^{2+} in the as-prepared catalyst disappeared when the potential reached 1.20 V vs. RHE, indicating that all the Co^{2+} species on the electrode surface had been converted to Co^{3+}. As the potential was further increased from 1.25 to 1.50 V vs. RHE the E$_g$ and F$_{2 g}$ peaks shifted to lower wavenumbers: from 468 and 511–446 and 493 cm^{-1}, respectively. As the A$_{1 g}$ peaks of Co^{3+} and Co^{4+} species of a Co-based electrocatalyst, such as Li$_{1-x}$CoO$_2$ (0.18 ≤ x ≤ 0.6) [70], appear in very similar wavenumbers, this peak cannot be used as an indicator of the Co^{3+}/Co^{4+} redox reaction. Nevertheless, the apparent shifts of the E$_g$ and F$_{2 g}$ peaks with the enhancement of applied potentials from 1.25 to 1.50 V vs. RHE provide important evidence for the oxidation of partial surface-Co^{3+} to Co^{4+} species.

Next, OCPT measurements were used to monitor the lifetimes of the electrogenerated Co^{3+} and Co^{4+} species on the DS-CoS NC surface. The measured open circuit potential (E_{OCP}) was used to identify the active species and reactions occurring on the working electrode surface (Fig. 3b). The OCPT experiment was conducted by applying a potential for 1 min and then switching off the potentiostat to measure the E_{OCP}. The initial Co^{2+} species yielded an E_{OCP} of 0.90 V vs. RHE. However, after the electrolysis at 1.05 V vs. RHE for 1 min, an E_{OCP} of 1.05 V vs. RHE was obtained, corresponding to the electrogenerated Co^{3+} species (Fig. 3b). The OCPT curve shows that the surface Co^{3+} species were spontaneously converted to Co^{2+} with a lifetime of approximately 1300 s. In addition, when electrolysis was carried out at 1.45 V vs. RHE for 1 min, an E_{OCP} of 1.45 V vs. RHE was observed, corresponding to the electrogenerated Co^{4+} species. The OCPT curve shows that Co^{4+} is spontaneously converted to Co^{2+} with a lifetime of approximately 5000 s. Notably, the Co^{4+} to Co^{2+} process could be divided into two
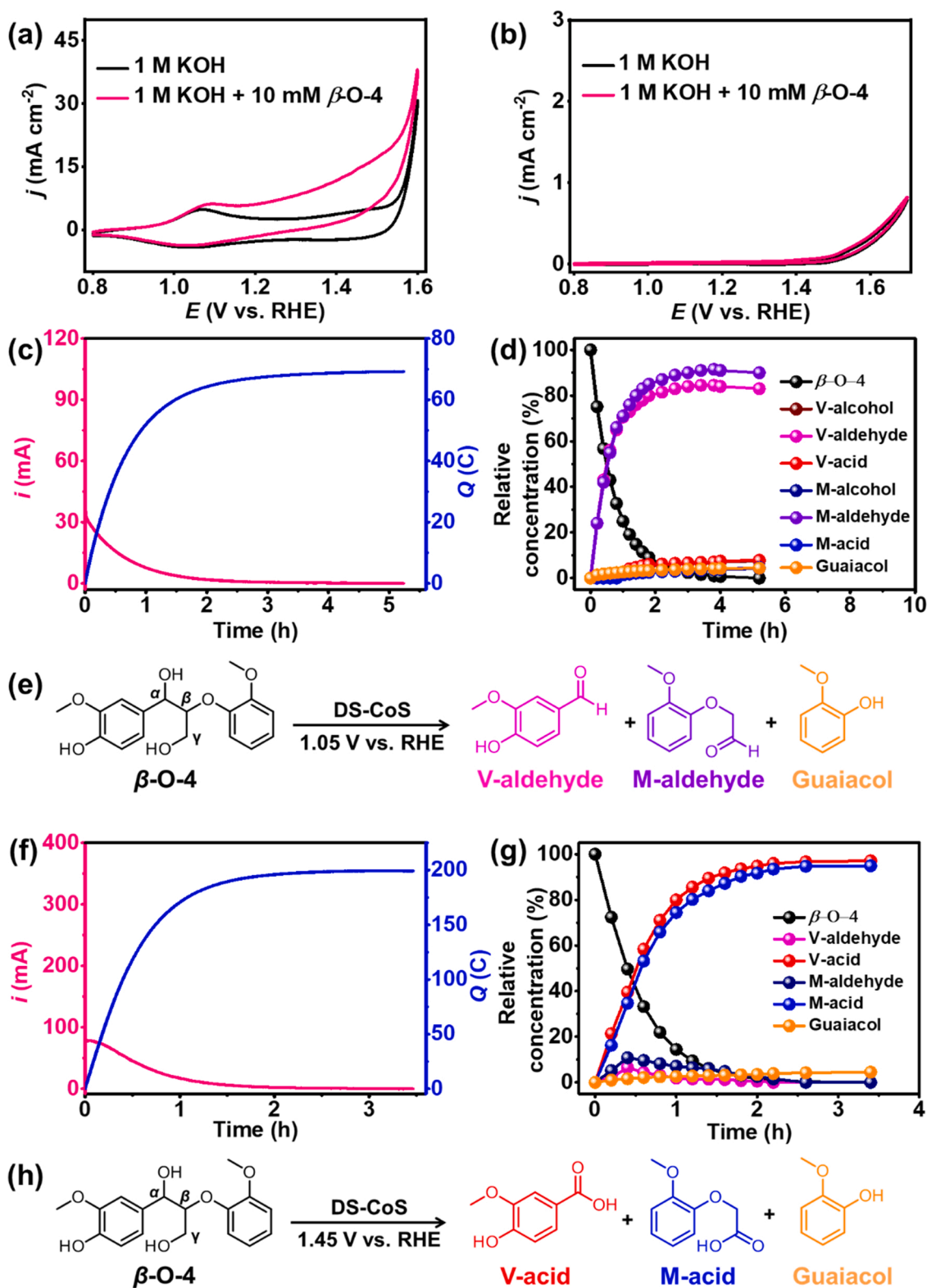
Fig. 2. (a) CVs of the DS-CoS nanocones in the presence and absence of 10 mM β-O-4 in 30 ml electrolyte. (b) CVs of glassy carbon in the presence and absence of 10 mM β-O-4 in 10 ml electrolyte (scan rate: 10 mv s^{-1}). (c) Chronoamperometry measurements at 1.05 V vs. RHE with 10 mM β-O-4 in 30 ml electrolyte. (d) Concentrations of β-O-4 and products versus reaction time obtained during chronoamperometry measurements at 1.05 V vs. RHE. (e) Scheme of the reaction during chronoamperometry at 1.05 V vs. RHE. (f) Chronoamperometry measurements at 1.45 V vs. RHE with 10 mM β-O-4 in 30 ml electrolyte. (g) Concentrations of β-O-4 and products versus reaction time obtained during chronoamperometry at 1.45 V vs. RHE. (h) Scheme of the reaction during chronoamperometry at 1.45 V vs. RHE.
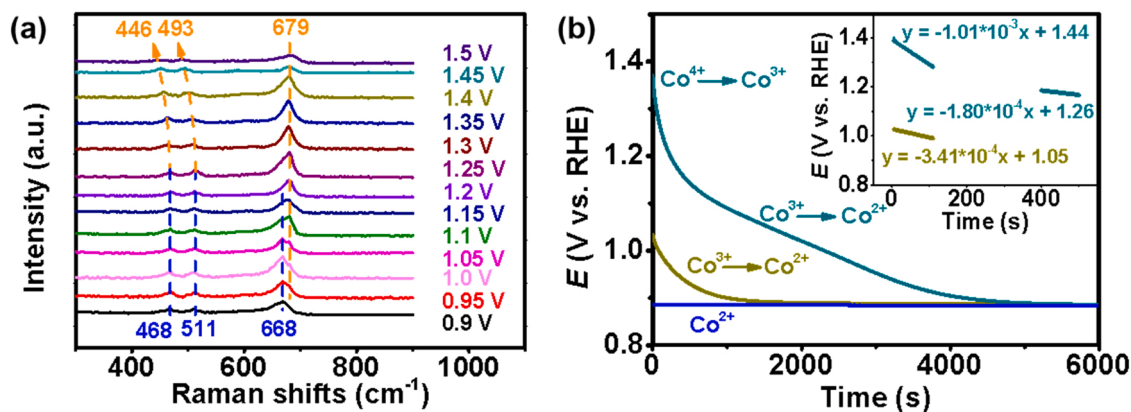
Fig. 3. (a) In situ electrochemical/Raman spectra of the DS-CoS nanocone surface recorded at applied potentials between 0.9 and 1.5 V vs. RHE. (b) Open-circuit potential versus time measurements to show the lifetimes of the electrogenerated Co^{3+} and Co^{4+} species on the surface of DS-CoS nanocones. The inset in (b) shows the rate of open-circuit voltage drop in OCPT.

steps based on the potential decay rate. It signifies that the electrogenerated Co^{4+} species were spontaneously converted to Co^{3+} and then to Co^{2+} species. The IERS and OCPT results showed that two electrogenerated intermediates, Co^{3+} and Co^{4+}, are involved in the electrocatalytic oxidation process. Specifically, the Co^{3+} species is responsible for the electrocatalytic C_α-C_β cleavage, whereas the Co^{4+} species for the further oxidation reactions of the cleavage products.

3.4. Mechanism of the C_α-C_β cleavage and oxygenation of β-O-4

The mechanism of the electrocatalytic C_α-C_β cleavage has not been systematically discussed in literatures [71,72]. To gain a deeper insight into the mechanism and to investigate the oxygen transfer process, isotope labeling experiments were carried out in $H_2^{18}O$ electrolyte under an argon atmosphere. When the electrolysis was conducted at 1.05 V vs. RHE, the mass spectrometry (MS) analysis of V-aldehyde indicated the formation of two products with molecular formulas (MFs) of $C_8H_8O_3$ and $C_8H_8O_2^{18}O$ in a ratio of 1.1:1 (Fig. S9a), and similarly the MS spectrum of M-aldehyde showed two products with MFs of $C_8H_{10}O_3$ and $C_8H_{10}O_2^{18}O$ almost in an equal amount (Fig. S9b).

Moreover, when the chronoamperometry experiment was carried out at 1.45 V vs. RHE, the V-acids with MFs of $C_8H_8O_3^{18}O$ and $C_8H_8O_2^{18}O_2$ were detected in a ratio of 1.05:1 (Fig. S10a), as were the M-acids with MFs of $C_8H_8O_3^{18}O$ and $C_8H_8O_2^{18}O_2$ in a ratio of 1: 1.05 (Fig. S10b). These results clearly indicate that water is the oxygen source, and the corresponding oxygen-containing active species may play a key role in the electrochemical process.

Hydroxyl and superoxide radicals are potential electrochemically generated active species that could drive the C_α-C_β cleavage reaction and further oxidation reactions [73–80]. Therefore, radical traps and electron spin resonance (ESR) methods are applied to detect the intermediates. *Tert*-butanol and *p*-benzoquinone, which are frequently used traps for hydroxyl and superoxide radicals, respectively, were adopted to study the C_α-C_β cleavage reaction of β-O-4 during the electrolysis at 1.05 V vs. RHE with the DS-CoS NC catalyst in 1 M KOH. It was found that the catalytic current dropped sharply and approached zero when *tert*-butanol was added to the electrolyte (Fig. S11a). This result indicates that hydroxyl radicals play a key role in the C_α-C_β cleavage reaction, and the surface electrogenerated Co^{3+} intermediate at 1.05 V vs. RHE could be $SCo^{3+}OH$. Furthermore, the ESR analysis is carried out to detect the spin reactive •OH and •O_2^- species on the catalyst surface and/or dissolved in water by using 5,5-dimethyl-1-pyrroline N-oxide (DMPO) as a spin trap. Typically, the strong ESR spectra with relative intensities of 1:2:2:1 correspond to DMPO-•OH, four significant characteristic peaks with identical intensity corresponding to the DMPO-•O_2^- [81]. Fig. S11b shows the spin-trapping ESR spectra

recorded at 1.05 V vs. RHE under electrolysis conditions with DMPO. The strong ESR spectra with relative intensities of 1:2:2:1 corresponding to DMPO-•OH adduct indicated the formation of •OH intermediate.

The electrooxidation of β-O-4 at 1.45 V vs. RHE is a two-step process that involves the C_α-C_β cleavage and further oxidation of the cleavage products. V-aldehyde and M-aldehyde are the main products of the C_α-C_β cleavage reaction. Therefore, V-aldehyde was chosen to study the mechanism of further oxidation at 1.45 V vs. RHE. When a sufficient quantity of *tert*-butanol was added to the electrolyte, there was a large increase in current, indicating that the oxidations of V-aldehyde and *tert*-butanol were not driven by hydroxyl radicals (Fig. S12a). As mentioned in some literatures [69–71], *p*-benzoquinone can be used to detect aqueous superoxide radicals. When *p*-benzoquinone was dissolved in the electrolyte, the V-aldehyde oxidation current at 1.45 V vs. RHE decreased to zero immediately (Fig. S12b), indicating that the electrochemically generated superoxide radicals were quenched by *p*-benzoquinone. Moreover, when the applied potential is controlled at 1.45 V vs. RHE, ESR spectra show four significant characteristic peaks with identical intensity (Fig. S12c), attributed to DMPO-•O_2^-, indicating the formation of •O_2^-. These results provide other pieces of evidence that the active species for further oxidation is most probably the electrogenerated $SCo^{4+}O$ on the surface of DS-CoS NCs.

On the basis of the above results, a plausible mechanism for the electrocatalytic oxidation of β-O-4 over the DS-CoS NCs is proposed as shown in Fig. 4a. First, the surface Co^{2+} on the DS-CoS nanocones is oxidized to $Co^{3+}OH$ at a low potential (1.05 V), which is accompanied by the generation of hydroxyl radicals. Subsequently, the hydroxyl radical abstracts an H-atom from C_α-OH of β-O-4 to form C_α-O• (**b**), which enables the cleavage of adjacent C—C bond via β-scission,[82–84] to form V-aldehyde (**c**) and intermediate **d** as shown in Fig. 4a. Density functional theory (DFT) calculations showed that the processes of the hydroxyl-radical attack and C_α-C_β cleavage take place readily, that is, with very low energy barriers (Fig. 4b). The further hydroxylation of the intermediate **d** has two possible pathways, depending on the hydroxylation site on C_β or C_γ. The DFT calculations revealed that the C_γ hydroxylation pathway (path 2 in Fig. 4a,b) is thermodynamically more favorable than the C_β hydroxylation pathway (path 1 in Fig. 4a,b). Along the reaction pathway, the radical rearrangement (TS-5, 46.25 kcal mol^{-1}) and HO-C_γ-OH dehydration (TS-6, 40.01 kcal mol^{-1}) have to overcome comparatively higher activation barriers. In the following process, V-aldehyde and M-aldehyde could be further oxidized to V-acid and M-acid, respectively, induced by the superoxide radicals formed over the electrogenerated Co^{4+} species. Furthermore, HPLC analysis showed that M-aldehyde and M-acid in electrolyte solutions spontaneously and gradually decomposed to guaiacol through C-O cleavage without requiring extra energy (Fig. S13).
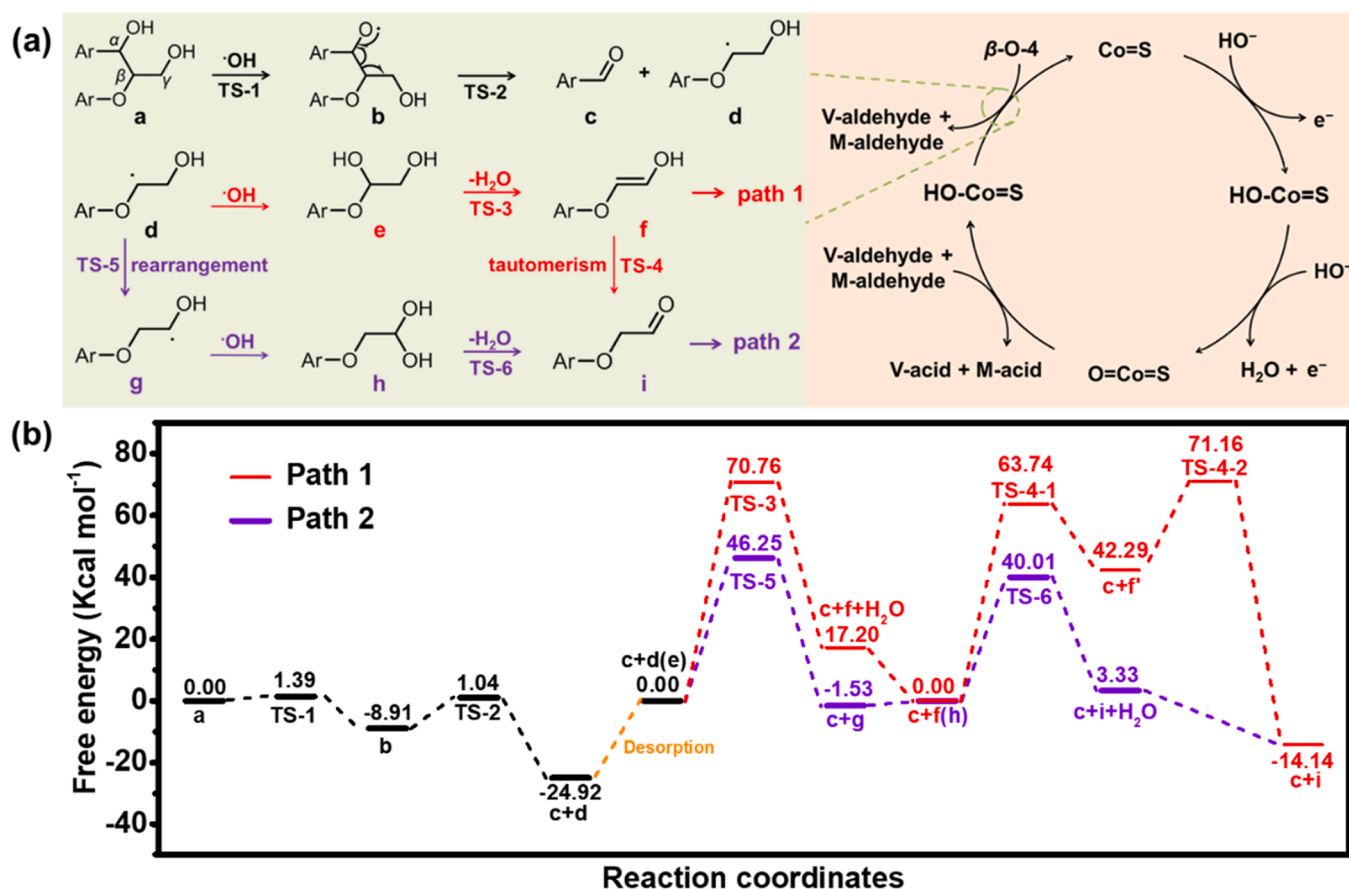
Fig. 4. (a) Proposed mechanism for the electrocatalytic oxidation of β-O-4 over DS-CoS nanocones. (b) Free energy diagram for the electrochemical oxidation of β-O-4.

3.5. Electrocatalytic oxidation of lignin

With the success in the electrocatalytic oxidation of β-O-4, we further studied the performance of the DS-CoS NCs for the electrocatalytic depolymerization of lignin. The chronoamperometry measurements were conducted in 1 M KOH at 1.05 and 1.45 V vs. RHE (Fig. 5a). Both number- and weight-average molecular weights (M_n and M_w, respectively) were monitored by gel permeation chromatography (GPC) to detect changes in the lignin, and low-molecular-weight products were detected by HPLC. The initial lignin had an M_n of 5.3 kDa and M_w of 17.5 kDa, and these decreased to 2.2 and 2.3 kDa, respectively, after electrolysis at 1.05 V vs. RHE for 25 h, and the M_n and M_w further decreased to 1.3 and 1.4 kDa, respectively, after electrolysis at 1.45 V vs. RHE for 16 h (Fig. S14). In the meantime, the color of the electrolyte changed from dark to brown. These results demonstrate that the DS-CoS NCs can electrocatalytically depolymerize lignin (Supporting Note 1). Moreover, 2D ^{1}H–^{13}C heteronuclear single quantum coherence (HSQC) NMR spectra of the lignin samples before and after oxidation provide further evidence for the conversion of polymer alcohol groups to the corresponding aldehydes at 1.05 V vs. RHE and then to carboxylic acids at 1.45 V vs. RHE (Fig. S15). In particular, the intensity of the signals corresponding to the α- and γ-hydrogen atoms of β-O-4 decreased for the oxidized lignin, accompanied by the appearance of a new signal corresponding to the β-hydrogen atoms of the oxidized β-O-4 moiety. HPLC analysis of the product mixtures corroborated the formation of significant quantities of various aromatic products (Figs. 5c and S16–18) with high depolymerization yields after electrolysis, 21.4 wt% (1.05 V vs. RHE) and 23.9 wt% (1.45 V vs. RHE) with respect to the original mass of lignin. The main molecular products obtained at 1.05 V vs. RHE were aldehydes, including benzyl (B)-, syringyl (S)-, and guaiacyl (G)-derived aldehydes. The main products generated at 1.45 V vs. RHE were carboxylic acids, including B-, S-, and G-derived carboxylic acids.

4. Conclusion

In summary, we demonstrated that the DS-CoS nanocones is an effective electrocatalyst that can selectively upgrade lignin and its derivative, β-O-4, to V-aldehyde and M-aldehyde through electrochemical oxidative C_α-C_β cleavage at 1.05 V vs. RHE. When the applied potential was higher than 1.25 V vs. RHE, the aldehydes were further oxidized to the corresponding carboxylic acids. In-depth mechanistic studies revealed that the hydroxyl radicals electrogenerated on the surface of SCo^{3+}OH induced the cleavage of the C_α-C_β bond, resulting in the formation of C_α carboxides and C_β radicals, which were rearranged to C_γ radicals and then oxidized to C_γ carboxides by electrophilic hydroxyl radicals. The further oxidation of the aldehydes to carboxylic acids is induced by superoxide radicals formed on the surface of the DS-CoS NCs. Crucially, monomeric aromatic aldehydes and carboxylates could be selectively produced with excellent yields by controlling the applied potential. This work provides a promising approach for the selective electrocatalytic oxidation of lignin and its derivatives through the C_α-C_β cleavage by employing non-noble metal catalysts under environmentally benign conditions without needing sacrificial oxidants.

CRediT authorship contribution statement

Z.F. designed the experiments, fabricated and analyzed the devices, carried out the TEM characterization, carried out, and analyzed the XPS measurements. F.L. and Q.T. contributed to the density functional theory calculations, revision and discussion of the paper. M.W., F.L., X.W.
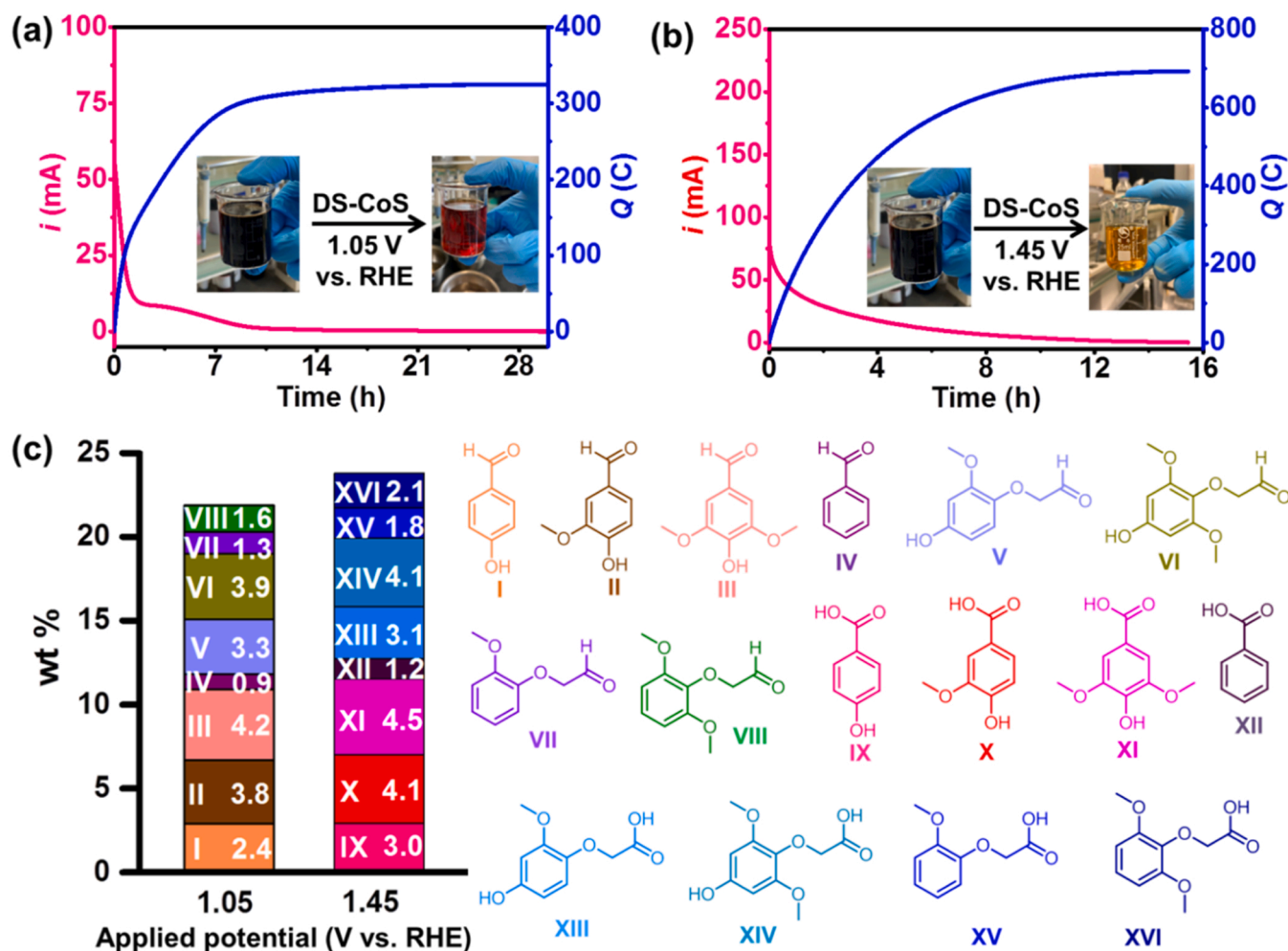
Fig. 5. Chronoamperometry measurements with 300 mg lignin at (a) 1.05 and (b) 1.45 V vs. RHE. (c) Weight percentages of aromatic monomers obtained from the depolymerization of lignin by chronoamperometry at 1.05 and 1.45 V vs. RHE.

and K.F. contributed to the revision and discussion of the paper. L.S. supervised the project and contributed to the revision and discussion of the paper. P.Z. designed the experiments, supervised the project, and wrote the paper.

Declaration of Competing Interest

The authors declare that they have no known competing financial interests or personal relationships that could have appeared to influence the work reported in this paper.

Data availability

Data will be made available on request.

Appendix A. Supplementary material

Supplementary data associated with this article can be found in the online version at doi:10.1016/j.apcatb.2022.122149.

References

[1] W. Boerjan, J. Ralph, M. Baucher, Lignin biosynthesis, Annu. Rev. Plant Biol. 54 (2003) 519–549.

[2] Z. Dou, Z. Zhang, M. Wang, Self-hydrogen transfer hydrogenolysis of native lignin over Pd-PdO/TiO$_2$, Appl. Catal. B Environ. 301 (2022), 120767.

[3] R. Vanholme, B. Demedts, K. Morreel, J. Ralph, W. Boerjan, Lignin biosynthesis and structure, Plant Physiol. 153 (2010) 895–905.

[4] B. Joffres, C. Lorentz, M. Vidalie, D. Laurenti, A.A. Quoineaud, N. Charon, A. Daudin, A. Quignard, C. Geantet, Catalytic hydroconversion of a wheat straw soda lignin: characterization of the products and the lignin residue, Appl. Catal. B Environ. 145 (2014) 167–176.

[5] M. Wang, F. Wang, Catalytic scissoring of lignin into aryl monomers, Adv. Mater. 31 (2019) 1901866.

[6] B. Joffres, M.T. Nguyen, D. Laurenti, C. Lorentz, V. Souchon, N. Charon, A. Daudin, A. Quignard, C. Geantet, Lignin hydroconversion on MoS$_2$-based supported catalyst: comprehensive analysis of products and reaction scheme, Appl. Catal. B Environ. 184 (2016) 153–162.

[7] J. Pu, T.-S. Nguyen, E. Leclerc, C. Lorentz, D. Laurenti, I. Pitault, M. Tayakout-Fayolle, C. Geantet, Lignin catalytic hydroconversion in a semi-continuous reactor: an experimental study, Appl. Catal. B Environ. 256 (2019), 117769.

[8] F. Yan, R. Ma, X. Ma, K. Cui, K. Wu, M. Chen, Y. Li, Ethanolysis of kraft lignin to platform chemicals on a MoC$_{1-x}$/Cu-MgAlO$_z$ catalyst, Appl. Catal. B Environ. 202 (2017) 305–313.

[9] B. Joffres, C. Lorentz, M. Vidalie, D. Laurenti, A.-A. Quoineaud, N. Charon, A. Daudin, A. Quignard, C. Geantet, Catalytic hydroconversion of a wheat straw soda lignin: characterization of the products and the lignin residue, Appl. Catal. B Environ. 145 (2014) 167–176.

[10] X. Dou, X. Jiang, W. Li, C. Zhu, Q. Liu, Q. Lu, X. Zheng, H. Chang, H. Jameel, Highly efficient conversion of Kraft lignin into liquid fuels with a Co-Zn-beta zeolite catalyst, Appl. Catal. B Environ. 268 (2020) 118429.

[11] S. Han, C. Wang, Y. Wang, Y. Yu, B. Zhang, Electrosynthesis of nitrate via the oxidation of nitrogen on tensile-strained palladium porous nanosheets, Angew. Chem. Int. Ed. 60 (2020) 4474–4478.

[12] S. Möhle, M. Zirbes, E. Rodrigo, T. Gieshoff, A. Wiebe, S.R. Waldvogel, Modern electrochemical aspects for the synthesis of value-added organic products, Angew. Chem. Int. Ed. 57 (2018) 6018–6041.

[13] C. Tang, Y. Zheng, M. Jaroniec, S.-Z. Qiao, Electrocatalytic refinery for sustainable production of fuels and chemicals, Angew. Chem. Int. Ed. 60 (2021) 19572–19590.

[14] M. Zirbes, S.R. Waldvogel, Electro-conversion as sustainable method for the fine chemical production from the biopolymer lignin, Curr. Opin. Green Sustain. Chem. 14 (2018) 19–25.

[15] M. Garedew, D. Young-Farhat, S. Bhatia, P. Hao, J.E. Jackson, C.M. SaffronL, Electrocatalytic cleavage of lignin model dimers using ruthenium supported on activated carbon cloth, Sustain, Energy Fuels 4 (2020) 1340.

[16] A. Vasileff, Y. Zhu, X. Zhi, Y. Zhao, L. Ge, H.M. Chen, Y. Zheng, S.-Z. Qiao, Electrochemical reduction of CO$_2$ to ethane through stabilization of an ethoxy intermediate, Angew. Chem. Int. Ed. 59 (2020) 19649–19653.

[17] X. Du, H. Zhang, K.P. Sullivan, P. Gogoi, Y. Deng, Electrochemical lignin conversion, ChemSusChem, 13 (202), pp. 4318–4343.

[18] M. Garedew, F. Lin, B. Song, T.M. DeWinter, J.E. Jackson, C.M. Saffron, C.H. Lam, P.T. Anastas, Greener routes to biomass waste valorization: lignin transformation through electrocatalysis for renewable chemicals and fuels production, ChemSusChem 13 (2020) 4214–4237.

[19] X. Wu, X. Fan, X. Sie, J. Lin, J. Cheng, Q. Zhang, L. Chen, Y. Wang, Solar energy-driven lignin-first approach to full utilization of lignocellulosic biomass under mild conditions, Nat. Catal. 1 (2018) 772–780.

[20] A. Rahimi, A. Ulbrich, J.J. Coon, S.S. Stahl, Formic-acid-induced depolymerization of oxidized lignin to aromatics, Nature 515 (2014) 249–252.

[21] W. Lan, J.B. Bueren, J. Luterbacher, Highly selective oxidation and depolymerization of α, γ-diol-protected lignin, Angew. Chem. Int. Ed. 58 (2019) 2649–2654.

[22] P. De Luna, C. Hahn, D. Higgins, S.A. Jaffer, T.F. Jaramillo, E.H. Sargent, What would it take for renewably powered electrosynthesis to displace petrochemical processes, Science 364 (2019) eaav3506.

[23] Y.X. Chen, A. Lavacchi, H.A. Miller, M. Bevilacqua, J. Filippi, M. Innocenti, A. Marchionni, W. Oberhauser, L. Wang, F. Vizza, Nanotechnology makes biomass electrolysis more energy efficient than water electrolysis, Nat. Commun. 5 (2014) 4036.

[24] S. Verma, S. Lu, P.J.A. Kenis, Co-electrolysis of CO$_2$ and glycerol as a pathway to carbon chemicals with improved technoeconomics due to low electricity consumption, Nat. Energy 4 (2019) 466–474.

[25] X. Wei, Y. Li, L. Chen, J. Shi, Formic acid electro-synthesis by concurrent cathodic CO$_2$ reduction and anodic CH$_3$OH oxidation, Angew. Chem. Int. Ed. 60 (2021) 3148–3155.

[26] V.L. Pardini, C.Z. Smith, J.H.P. Utley, R.R. Vargas, H. Viertler, Electroorganic reactions. 38. Mechanism of electrooxidative cleavage of lignin model dimers, J. Org. Chem. 56 (1991) 7305–7313.

[27] S. Stiefel, A. Schmitz, J. Peters, D.D. Di Marino, M. Wessling, An integrated electrochemical process to convert lignin to valueadded products under mild conditions, Green Chem. 18 (2016) 4999–5007.

[28] P. Cai, H. Fan, S. Cao, J. Qi, S. Zhang, G. Li, Electrochemical conversion of corn stover lignin to biomass-based chemicals between Cu/Ni-Mo-Co cathode and Pb/PbO$_2$ anode in alkali solution, Electrochim. Acta 264 (2018) 128–139.

[29] Y.-S. Wang, F. Yang, Z.-H. Liu, L. Yuan, G. Li, Electrocatalytic degradation of aspen lignin over Pb/PbO$_2$ electrode in alkali solution, Catal. Commun. 67 (2015) 49–53.

[30] Y. Jia, Y. Wen, X. Han, J. Qi, Z. Liu, S. Zhang, G. Li, Electrocatalytic degradation of rice straw lignin in alkaline solution through oxidation on a Ti/SnO$_2$-Sb$_2$O$_3$/α-PbO$_2$/β-PbO$_2$ anode and reduction on an iron or tin doped titanium cathode, Catal. Sci. Technol. 8 (2018) 4665–4677.

[31] Y. Zhang, Y. Peng, X. Yin, Z. Liu, G. Li, Degradation of lignin to BHT by electrochemical catalysis on Pb/PbO$_2$ anode in alkaline solution, J. Chem. Technol. Biotechnol. 89 (2014) 1954–1960.

[32] Z. Lu, B. Tu, F. Chen, Electro-degradation of sodium lignosulfonate, J. Wood Chem. Technol. 23 (2003) 261–277.

[33] P. Parpot, A. Bettencourt, A. Carvalho, E. Belgsir, Biomass conversion: attempted electrooxidation of lignin for vanillin production, J. Appl. Electrochem. 30 (2000) 727–731.

[34] X. Hao, Y. Quansheng, S. Dan, Y. Honghui, L. Jidong, F. Jiangtao, Y. Wei, Fabrication and characterization of PbO$_2$ electrode modified with [Fe(CN)6]3– and its application on electrochemical degradation of alkali lignin, J. Hazard. Mater. 286 (2015) 509–516.

[35] D. Shao, J. Liang, X. Cui, H. Xu, W. Yan, Electrochemical oxidation of lignin by two typical electrodes: Ti/SbSnO$_2$ and Ti/PbO$_2$, Chem. Eng. J. 244 (2014) 288–295.

[36] X. Chang, J. Zalm, S.S. Thind, A. Chen, Electrochemical oxidation of lignin at electrochemically reduced TiO$_2$ nanotubes, J. Electroanal. Chem. 863 (2020) 14049.

[37] V.L. Pardini, R.R. Vargas, H. Viertler, J.H. Utley, Anodic cleavage of lignin model dimers in methanol, Tetrahedron 48 (1992) 7221–7228.

[38] O. Movil-Cabrera, A. Rodriguez-Silva, C. Arroyo-Torres, J.A. Staser, Electrochemical conversion of lignin to useful chemicals, Biomass Bioenergy 88 (2016) 89–96.

[39] L. Ma, H. Zhou, X. Kong, Z. Li, H. Duan, An electrocatalytic strategy for C−C bond cleavage in lignin model compounds and lignin under ambient conditions, ACS Sustain. Chem. Eng. 9 (2021) 1932–1940.

[40] R. Tolba, M. Tian, J. Wen, Z.-H. Jiang, A. Chen, Electrochemical oxidation of lignin at IrO$_2$-based oxide electrodes, J. Electroanal. Chem. 649 (2010) 9–15.

[41] E. Reichert, R. Wintringer, D.A. Volmer, R. Hempelmann, Electro-catalytic oxidative cleavage of lignin in a protic ionic liquid, Phys. Chem. Chem. Phys. 14 (2012) 5214–5221.

[42] L. Wang, Y. Chen, S. Liu, H. Jiang, L. Wang, Y. Sun, P. Wan, Study on the cleavage of alkyl-O-aryl bonds by in situ generated hydroxyl radicals on an ORR cathode, RSC Adv. 7 (2017) 51419–51425.

[43] M. Tian, J. Wen, D. MacDonald, R.M. Asmussen, A. Chen, A novel approach for lignin modification and degradation, Electrochem. Commun. 12 (2010) 527–530.

[44] D. Rauber, T.K. Dier, D.A. Volmer, R. Hempelmann, Electrochemical lignin degradation in ionic liquids on ternary mixed metal electrodes, Z. Phys. Chem. 232 (2018) 189–208.

[45] H. Zhu, Y. Chen, T. Qin, L. Wang, Y. Tang, Y. Sun, P. Wan, Lignin depolymerization via an integrated approach of anode oxidation and electro-generated H$_2$O$_2$ oxidation, RSC Adv. 4 (2014) 6232–6238.

[46] H. Zhu, L. Wang, Y. Chen, G. Li, H. Li, Y. Tang, P. Wan, Electrochemical depolymerization of lignin into renewable aromatic compounds in a non-diaphragm electrolytic cell, RSC Adv. 4 (2014) 29917–29924.

[47] T. Cui, L. Ma, S. Wang, C. Ye, X. Liang, Z. Zhang, G. Meng, L. Zheng, H.-S. Hu, J. Zhang, H. Duan, D. Wang, Y. Li, Atomically dispersed Pt−N$_3$C$_1$ sites enabling efficient and selective electrocatalytic C−C bond cleavage in lignin models under ambient conditions, J. Am. Chem. Soc. 143 (2021) 9429–9439.

[48] M. Rafiee, M. Alherech, S.D. Karlen, S.S. Stahl, Electrochemical aminoxyl-mediated oxidation of primary alcohols in lignin to carboxylic acids: polymer modification and depolymerization, J. Am. Chem. Soc. 141 (2019) 15266–15276.

[49] A. Rahimi, A. Azarpira, H. Kim, J. Ralph, S.S. Stahl, Chemoselective metal-free aerobic alcohol oxidation in lignin, J. Am. Chem. Soc. 135 (2013) 6415–6418.

[50] D. Rochefort, R. Bourbonnais, D. Leech, M.G. Paice, Oxidation of lignin model compounds by organic and transition metal-based electron transfer mediators, Chem. Commun. (2002) 1182–1183.

[51] T. Shiraishi, Y. Sannami, H. Kamitakahara, T. Takano, Comparison of a series of laccase mediators in the electro-oxidation reactions of non-phenolic lignin model compounds, Electrochim. Acta 106 (2013) 440–446.

[52] Y.S. Choi, R. Singh, J. Zhang, G. Balasubramanian, M.R. Sturgeon, R. Katahir, G. Chupk, G.T. Beckham, B.H. Shanks, Pyrolysis reaction networks for lignin model compounds: unraveling thermal deconstruction of β-O-4 and α-O-4 compounds, Green Chem. 18 (2016) 1762.

[53] M. Dawange, M.V. Galkin, J.S.M. Samec, Selective aerobic benzylic alcohol oxidation of lignin model compounds: route to aryl ketones, ChemCatChem 7 (2015) 401–404.

[54] N. Luo, M. Wang, H. Li, J. Zhang, T. Hou, H. Chen, X. Zhang, J. Lu, F. Wang, Visible-light-driven self-hydrogen transfer hydrogenolysis of lignin models and extracts into phenolic products, ACS Catal. 7 (2017) 4571–4580.

[55] P. Picart, C. Mller, J. Mottweiler, L. Wiermans, C. Bolm, P.D. Maria, A. Schallmey, From gene towards selective biomass valorization: bacterial b-etherases with catalytic activity on lignin-like polymers, ChemSusChem 7 (2014) 3164–3171.

[56] L. Wang, Z.H. Dong, Z.G. Wang, F.X. Zhang, J. Jin, Layered α-Co(OH)$_2$ nanocones as electrode materials for pseudocapacitors: understanding the effect of interlayer space on electrochemical activity, Adv. Funct. Mater. 23 (2013) 2758–2764.

[57] X. Liu, R. Ma, Y. Bando, T. Sasaki, Layered cobalt hydroxide nanocones: microwave-assisted synthesis, exfoliation, and structural modification, Angew. Chem. Int. Ed. 49 (2010) 8253–8256.

[58] A.-Y. Park, H. Kwon, A.J. Woo, S.-J. Kim, Layered double hydroxide surface modified with (3-aminopropyl) triethoxysilane by covalent bonding, Adv. Mater. 17 (2005) 106–109.

[59] E.L. Crepaldi, P.C. Pavan, J.B. Valim, Anion exchange in layered double hydroxides by surfactant salt formation, J. Mater. Chem. 10 (2000) 1337–1343.

[60] M.J.T. Frisch, G.W. Schlegel, H.B. Scuseria, G.E. Robb, M.A. Cheeseman, J.R. Scalmani, G. Barone, V. Petersson, G.A. Nakatsuji, H. Li, X. Caricato, M. Marenich, A.V. Bloino, J. Janesko, B.G. Gomperts, R. Mennucci, B. Hratchian, H.P. Ortiz, J.V. Izmaylov, A.F. Sonnenberg, J.L. Williams-Young, D. Ding, F. Lipparini, F. Egidi, F. Goings, J. Peng, B. Petrone, A. Henderson, T. Ranasinghe, D. Zakrzewski, V.G. Gao, J. Rega, N. Zheng, G. Liang, W. Hada, M. Ehara, M. Toyota, K. Fukuda, R. Hasegawa, J. Ishida, M. Nakajima, T. Honda, Y. Kitao, O. Nakai, H. Vreven, T. Throssell, K. Montgomery, J.A. Jr. Peralta, J.E. Ogliaro, F. Bearpark, M.J. Heyd, J. J. Brothers, E.N. Kudin, K.N. Staroverov, V.N. Keith, T.A. Kobayashi, R. Normand, J. Raghavachari, K. Rendell, A.P. Burant, J.C. Iyengar, S.S. Tomasi, J. Cossi, M. Millam, J.M. Klene, M. Adamo, C. Cammi, R. Ochterski, J.W. Martin, R.L. Morokuma, K. Farkas, O. Foresman, J.B. Fox, D.J., Gaussian 16. Gaussian Inc.: Wallingford, CT, 2016.

[61] A.D. Becke, Density-functional exchange-energy approximation with correct asymptotic-behavior, Phys. Rev. A 38 (1988) 3098–3100.

[62] C.T. Lee, W.T. Yang, R.G. Parr, Development of the colle-salvetti correlation-energy formula into a functional of the electron-density, Phys. Rev. B. 37 (1988) 785–789.

[63] M. Fleischmann, K. Korinek, D. Pletcher, The kinetics and mechanism of the oxidation of amines and alcohols at oxide-covered nickel, silver, copper, and cobalt electrodes, J. Chem. Soc. Perkin Trans. 10 (1972) 1396–1403.

[64] P. Zhang, X. Sheng, X. Chen, Z. Fang, J. Jiang, M. Wang, F. Li, L. Fan, Y. Ren, B. Zhang, B.J.J. Timmer, M.S.G. Ahlquist, L. Sun, Paired electrocatalytic oxygenation and hydrogenation of organic substrates using water as oxygen and hydrogen source, Angew. Chem. Int. Ed. 58 (2019) 9155–9159.

[65] M.T. Bender, Y.C. Lam, S. Hammes-Schiffer, K.-S. Choi, Unraveling two pathways for electrochemical alcohol and aldehyde oxidation on NiOOH, J. Am. Chem. Soc. 142 (2020) 21538–21547.

[66] Z. Fang, P. Zhang, M. Wang, F. Li, X. Wu, K. Fan, L. Sun, Selective electro-oxidation of alcohols to the corresponding aldehydes in aqueous solution via Cu(III) intermediates from CuO nanorods, ACS Sustain. Chem. Eng. 9 (2021) 11855–11861.

[67] D. Ma, B. Hu, W. Wu, X. Liu, J. Zai, C. Shu, T.T. Tsega, L. Chen, X. Qian, T.L. Liu, Highly active nanostructured CoS₂/CoS heterojunction electrocatalysts for aqueous polysulfide/iodide redox flow batteries, Nat. Commun. 10 (2019) 3367.

[68] S. Peng, X. Han, L. Li, Z. Zhu, F. Cheng, M. Srinivansan, S. Adams, S. Ramakrishna, Unique cobalt sulfide/reduced graphene oxide composite as an anode for sodium-ion batteries with superior rate capability and long cycling stability, Small 12 (2016) 1359–1368.

[69] C.-Y. Chen, Z.-Y. Shih, Z. Yang, H.-T. Chang, Carbon nanotubes/cobalt sulfide composites as potential high-rate and high-efficiency supercapacitors, J. Power Sources 215 (2012) 43–47.

[70] M. Inaba, Y. Iriyama, Z. Ogumi, Y. Todzuka, A. Tasaka, Raman study of layered rock-salt LiCoO2 and its electrochemical lithium deintercalation, J. Raman Spectrosc. 28 (1997) 613–617.

[71] A.A. Dallea, L. Domerguea, F. Fourcadea, A.A. Assadia, H. Djelala, T. Lendormic, I. Soutrela, S. Tahab, A. Amrane, Efficiency of DMSO as hydroxyl radical probe in an electrochemical advanced oxidation process reactive oxygen species monitoring and impact of the current density, Electrochim. Acta 246 (2017) 1–8.

[72] T.A. Enache, A.-M. Chiorcea-Paquim, F.-F. Orlando, A.M. Oliveira-Brett, Hydroxyl radicals electrochemically generated in situ on a boron-doped diamond electrode, Electrochem. Commun. 11 (2019) 1342–1345.

[73] Y. Huang, J. Zhou, D. Zhan, Z. Tian, Exploring the concentration distribution of photo-generated hydroxyl radicals in a confined etchant layer by scanning electrochemical microscopy, Electrochim. Acta 258 (2017) 322–327.

[74] D. Surachet, D.-S. Kim, T.L. Phares, C.-H. Li, J.R. Jinschek, A.C. Alba-Rubio, Supersensitive CeOx-based nanocomposite sensor for the electrochemical detection of hydroxyl free radicals, Nanoscale 13 (2021) 5136–5144.

[75] Z. Ma, B. Zhao, Z. Yuan, Application of electrochemical and spin trapping techniques in the investigation of hydroxyl radicals, Anal. Chim. Acta 389 (1999) 213–218.

[76] L.E. Manring, M.K. Kramer, C.S. Foote, Interecpyion of O_2^- by benzoquinone in cyanoaromatic-sensitized photooxygenation, Tetrahedron Lett. 25 (1984) 2523–2526.

[77] J.P. Lopez, The Interaction of O_2^- with water, Chem. Phys. Lett. 125 (1986) 454–458.

[78] A. Maroz, O. Brede, Reaction of radicals with benzoquinone-addition or electron transfer, Radiat. Phys. Chem. 67 (2003) 275–278.

[79] Y.-J. Chen, T. Lei, H.-L. Hu, H.-L. Wu, S. Zhou, X.-B. Li, B. Chen, C.-H. Tung, L.-Z. Wu, Tandem photoelectrochemical and photoredox catalysis for efficient and selective aryl halides functionalization by solar energy, Matter 4 (2021) 2354–2366.

[80] X.-B. Li, Z.-K. Xin, S.-G. Xia, X.-Y. Gao, C.-H. Tung, L.-Z. Wu, Semiconductor nanocrystals for small molecule activation via artificial photosynthesis, Chem. Soc. Rev. 49 (2020) 9028–9056.

[81] Z. Jiang, W. Wan, H. Li, S. Yuan, H. Zhao, P.K. Wong, A hierarchical Z-scheme α-Fe₂O₃/g-C₃N₄ hybrid for enhanced photocatalytic CO₂ reduction, Adv. Mater. 30 (2018) 1706108.

[82] X.-Y. Yu, J.-R. Chen, W.-J. Xiao, Visible light-driven radical-mediated C−C bond cleavage/functionalization in organic synthesis, Chem. Rev. 121 (2021) 506–561.

[83] H.G. Yayla, H. Wang, K.T. Tarantino, H.S. Orbe, R.R. Knowles, Catalytic ring-opening of cyclic alcohols enabled by PCET activation of strong O−H bonds, J. Am. Chem. Soc. 138 (2016) 10794–10797.

[84] Y. Wang, Y. Liu, J. He, Y. Zhang, Redox-neutral photocatalytic strategy for selective C−C bond cleavage of lignin and lignin models via PCET process, Sci. Bull. 64 (2019) 1658–1666.